Optimizing *n*-type doping of $ZnGeN_2$ and $ZnSiN_2$

Nicholas L. Adamski,[1,*] Zhen Zhu,[2,†] Darshana Wickramaratne,[2,3] and Chris G. Van de Walle[2]
[1]*Department of Electrical and Computer Engineering, University of California, Santa Barbara, California 93106-9560, USA*
[2]*Materials Department, University of California, Santa Barbara, California 93106-5050, USA*
[3]*Center for Computational Materials Science, US Naval Research Laboratory, Washington, DC 20375, USA*

(Received 12 August 2019; revised manuscript received 4 October 2019; published 30 October 2019)

In order for the wide-band-gap Zn-IV-nitrides to find applications in power electronics or optoelectronics, controlled *n*-type doping is required. We systematically explore group-V and group-VI dopants that can act as donors in $ZnGeN_2$ and $ZnSiN_2$. We address compensation by native acceptors as well as self-compensation by formation of *DX* centers. For $ZnGeN_2$, we find that S_N, Se_N, P_{Ge}, and As_{Ge} act as shallow donors. P_{Ge} has the lowest formation energy and can be used to reach carrier concentrations up to $n = 1.3 \times 10^{19}$ cm^{-3}. P_{Si} acts as a shallow donor in $ZnSiN_2$; however, because of strong compensation from native acceptors, we find that $ZnSiN_2$ cannot be doped *n* type.

DOI: 10.1103/PhysRevB.100.155206

I. INTRODUCTION

The Zn-IV-nitrides are a class of wide-band-gap semiconductors that are being examined for applications in solar cells [1], light-emitting diodes [2], and high-power electronics [3]. With a structure similar to the wurtzite structure, there is potential for integrating Zn-IV-nitrides into devices with III-nitrides [4]. All of these applications require controllable *n*-type doping.

The band gaps of the Zn-IV-nitrides range from 1.4 eV for $ZnSnN_2$ to 3.3 eV for $ZnGeN_2$ up to 4.5 eV for $ZnSiN_2$ [3,5,6]. $ZnSnN_2$ is reported to be degenerately *n*-type doped, with carrier concentrations on the order of 10^{20}–10^{21} cm^{-3} [6–8], while growth of $ZnGeN_2$ [9,10] and $ZnSiN_2$ [11] typically results in insulating material. O_N dopants and Sn_{Zn} antisites have been identified as likely sources of *n*-type conductivity in $ZnSnN_2$ [12,13]. Previous theoretical work on $ZnGeN_2$ using density functional theory (DFT) has shown that O_N acts as a shallow donor and the Ge_{Zn} antisite acts as a deep donor; however, they are heavily compensated by Zn_{Ge} antisite and V_{Zn} vacancy defects that act as acceptors [14,15]. We are not aware of any studies of defects or doping in $ZnSiN_2$. To determine if $ZnGeN_2$ and $ZnSiN_2$ can be intentionally *n*-type doped, we examine a variety of donors and evaluate the effect of compensation from native acceptors.

DX behavior poses a challenge for *n*-type doping in wide-band-gap semiconductors. A *DX* center occurs when a donor impurity undergoes a large lattice relaxation and captures two electrons, in the process converting to an acceptor. For example, Si_{Ga} acts as a shallow donor in GaN, but for $Al_xGa_{1-x}N$ with high Al concentration, silicon has a transition level between the positive and negative charge states that lies within the band gap [16]. As a result, it is difficult to achieve high carrier concentrations in $Al_xGa_{1-x}N$ [17]. With a different set of potential donors, the Zn-IV-nitrides could potentially enable levels of *n*-type doping that are difficult to achieve in $Al_xGa_{1-x}N$.

To obtain *n*-type conductivity, we search for dopants with a strong preference for substitution on a specific site. If the dopant substitutes on the wrong site, it may contribute to compensation. Group-III dopants, such as Al, Ga, and In, may suffer from self-compensation as they are likely to substitute both on the Zn site as a donor, and on the group-IV site as a compensating acceptor [18]. O has been investigated as an unintentional dopant, where it substitutes as a donor on the N site [15]. Similarly, S and Se can be expected to preferentially substitute on the N site [16]. We also consider P and As, which can substitute as donors on the cation site and are isoelectronic with nitrogen.

Using DFT with a hybrid functional, we investigate P, As, S, and Se as dopants substituting on each potential site in $ZnGeN_2$ and $ZnSiN_2$. We compare the formation energies of these dopants acting as donors with their formation energies when incorporating on competing sites. Since the concentrations of the donors as well as the native acceptors depend on the growth conditions, we calculate the *n*-type carrier concentration for a range of growth conditions to determine the effect of compensation and select the optimal donor for achieving *n*-type conductivity.

II. COMPUTATIONAL METHODS

Calculations are performed using DFT with projector augmented wave potentials [19] as implemented in the Vienna *Ab initio* Simulation Package (VASP) [20,21]. We use the hybrid functional of Heyd, Scuseria, and Ernzerhof (HSE) [22,22] with a standard mixing parameter of 25%. $ZnGeN_2$ and $ZnSiN_2$ have orthorhombic symmetry with the $Pna2_1$ space group. The primitive unit cell contains 16 atoms [15]. Our calculated lattice parameters for $ZnGeN_2$ and $ZnSiN_2$, listed in Table I, agree well with experimental values [23,24].

*nadamski@ucsb.edu
†Present address: Google LLC, 1600 Amphitheatre Parkway, Mountain View, California, USA.

TABLE I. Calculated and experimental lattice parameters of $ZnGeN_2$ and $ZnSiN_2$.

$ZnGeN_2$	a (Å)	b (Å)	c (Å)
HSE	5.47	6.45	5.20
Expt. (Ref. [23])	5.45	6.44	5.19
$ZnSiN_2$			
HSE	5.24	6.27	5.02
Expt. (Ref. [24])	5.25	6.28	5.02

$ZnGeN_2$ has a direct band gap at the Γ point calculated to be 3.19 eV [15]. $ZnSiN_2$ has an indirect band gap of 4.83 eV: the conduction-band minimum (CBM) is at Γ, while the valence-band maximum (VBM) is at T. The band structures of $ZnGeN_2$ and $ZnSiN_2$ are plotted in Fig. 1. Punya *et al.* previously calculated the band structure of $ZnGeN_2$ and $ZnSiN_2$ using the quasiparticle self-consistent GW approximation [25]. For $ZnGeN_2$, they found a direct band gap of 3.42 eV, while for $ZnSiN_2$, they found an indirect band gap of 5.44 eV with the VBM residing between Γ and X. We find the same local maxima in the valence band but find the maximum at the T point to be higher than the local maximum between Γ and X. The difference is small (less than 0.2 eV), however, and mostly results from differences in the lattice parameters. Note that there is a difference in the labeling of **k** points between our results and the results of Punya *et al.* as they interchanged the a and b lattice vectors.

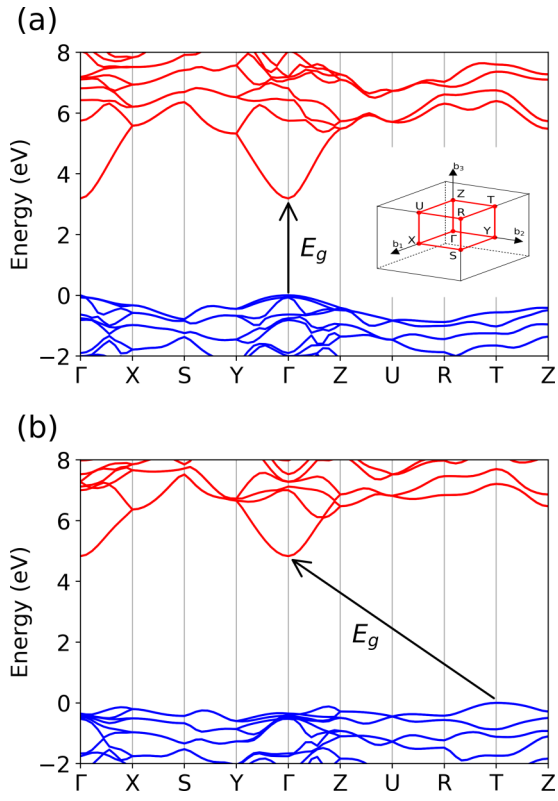

FIG. 1. Calculated band structure of (a) $ZnGeN_2$ and (b) $ZnSiN_2$. Inset: Brillouin zone for the orthorhombic lattice.

TABLE II. Formation enthalpies for $ZnGeN_2$, $ZnSiN_2$, and limiting phases.

Compound	Calc. (eV)	Expt. (eV)	Reference
$ZnGeN_2$	−1.09		
$ZnSiN_2$	−3.71		
Zn_3N_2	+0.20	−0.25	Ref. [29]
Ge_3N_4	−0.77	−0.64	Ref. [30]
Si_3N_4	−8.83	−8.58	Ref. [31]
ZnS	−1.88	−2.12	Ref. [32]
ZnSe	−1.73	−1.84	Ref. [32]
P_3N_5	−3.87	−3.32	Ref. [33]
Zn_3P_2	−1.28	−1.71	Ref. [34]
Zn_3As_2	−1.29	−1.34	Ref. [35]
GeAs	−0.13		
$ZnGeAs_2$	−0.93		
ZnO	−3.10	−3.62	Ref. [29]
GeO_2	−4.93	−5.70	Ref. [29]
SiO_2	−8.90	−9.44	Ref. [33]

Defect calculations are performed in a $2 \times 2 \times 2$ supercell with 128 atoms using a $2 \times 2 \times 2$ k-point mesh [resulting in the single special **k** point (1/4, 1/4, 1/4)]. Convergence tests showed that the formation energies change by less than 0.01 eV when a $4 \times 4 \times 4$ mesh is used. Spin polarization was included in all calculations.

The formation energy of a defect D in charge state q is defined as [26]

$$E^f(D^q) = E_{\text{tot}}(D^q) - E_{\text{tot}}(\text{bulk}) + \sum_i n_i \mu_i + qE_F + \Delta^q, \tag{1}$$

where $E_{\text{tot}}(D^q)$ is the energy of the supercell with the defect in the charge state q, $E_{\text{tot}}(\text{bulk})$ is the energy of the pristine supercell structure, and μ_i is the chemical potential of the atoms added or removed to form the defect. E_F is the Fermi energy, referenced to the VBM, and Δ^q is the Freysoldt correction [27,28].

The chemical potentials are variables that reflect the growth conditions; for $ZnGeN_2$, these are reflected in the choice of chemical potentials for Zn, Ge, and N [26]. The chemical potentials are constrained by equilibrium with $ZnGeN_2$:

$$\Delta H^f(ZnGeN_2) = \Delta\mu_{Zn} + \Delta\mu_{Ge} + 2\Delta\mu_N, \tag{2}$$

where $\Delta H^f(ZnGeN_2)$ is the enthalpy of formation of $ZnGeN_2$. The chemical potentials of Zn, Ge, and N are referenced to their elemental form; for instance, $\mu_{Zn} = \mu_{Zn(\text{bulk})} + \Delta\mu_{Zn}$. Similar equations hold for the chemical potentials in $ZnSiN_2$. The choice of chemical potentials for dopants is constrained by equilibrium with the host structure and by the formation of competing phases. The calculated formation enthalpies of $ZnGeN_2$ and $ZnSiN_2$, along with the formation enthalpies of the limiting phases, are compared with experimental values in Table II. Phase stability diagrams are plotted in Fig. 2. We highlight the extrema of the $ZnGeN_2$ and $ZnSiN_2$ stability regions as they will be convenient choices of chemical potentials for plotting formation energies.

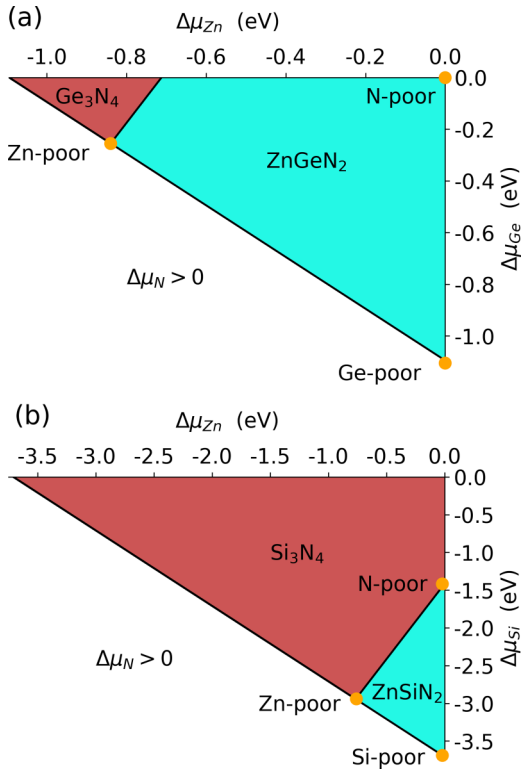

FIG. 2. The calculated phase stability diagrams for (a) $ZnGeN_2$ and (b) $ZnSiN_2$.

To evaluate each dopant, we determine the maximum carrier concentration that can be induced in each material. In equilibrium, the total number of positive and negative charges in the material will be equal. The positive charges in the material are the free holes and positively charged point defects or impurities, while the negative charges are the free electrons and negatively charged point defects or impurities. For n-type material, the hole concentration p is small and can be neglected. The concentration of charge Q resulting from a particular defect or impurity i is

$$Q_i = q_i N_{\text{sites}} \exp\left(\frac{-E_i^f}{k_B T}\right), \tag{3}$$

where q_i is the charge of the defect or impurity, N_{sites} is the concentration of sites it can occupy, E_i^f is the formation energy, k_B is Boltzmann's constant, and T is the growth temperature. This expression is summed over all point defects and impurities in the system. The full charge balance equation in equilibrium can be written as

$$\sum_i q_i N_{\text{sites}} \exp\left(\frac{-E_i^f}{k_B T}\right) = N_c \exp\left(\frac{-E_F}{k_B T}\right), \tag{4}$$

where the electron concentration n is expressed assuming the Boltzmann approximation (nondegenerate limit) and N_c is the effective density of states for the conduction band.

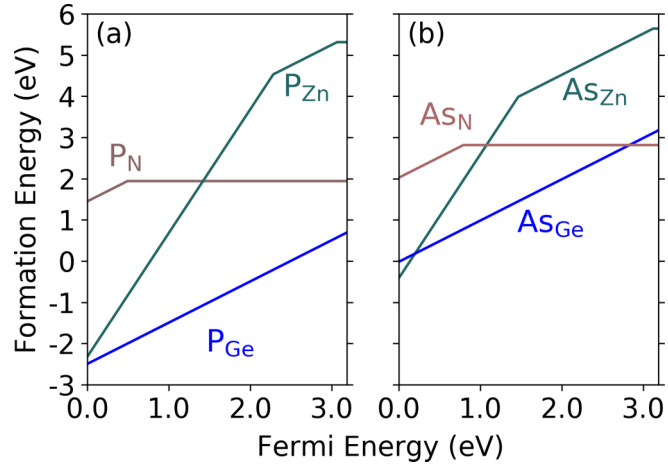

FIG. 3. Formation energies for (a) P and (b) As substitutional impurities in $ZnGeN_2$ under N-poor conditions.

III. RESULTS

A. $ZnGeN_2$

As $ZnGeN_2$ is a ternary material, there are three types of substitutional impurities that can result in (single) donors: substitution of a group-III element on the Zn site, substitution of a group-V element on the Ge site, or substitution of a group-VI element on the N site. For the group-III elements we have previously published work examining Al, Ga, and In, finding that they substitute both as a donor on the Zn site and as an acceptor on the Ge site [18]. This strong tendency for self-compensation renders it difficult (or impossible) to obtain n-type doping with group-III elements. We will therefore focus on group-V and group-VI dopants. We will first examine the properties of each of the substitutional dopants, and then evaluate the carrier concentrations that can be achieved.

1. Group-V donors: P and As

In Fig. 3, we plot the formation energies as a function of Fermi level for P and As substituting on each of the Zn, Ge, or N sites. The group-V elements are expected to act as donors when substituting on the Ge site. Indeed, we find that P_{Ge} and As_{Ge} act as shallow donors (i.e., the positive charge state is the only stable charge state over the entire range of Fermi levels). For both P_{Ge} and As_{Ge}, the $(+/0)$ and $(0/-)$ transition levels occur well above the CBM, indicating that neither impurity exhibits DX-center behavior.

P_{Ge} and As_{Ge} also have relatively low formation energies. However, P and As can also substitute on the Zn or N sites, and the effects of incorporation on those sites need to be examined. On the Zn site, P and As should still act as donors (expected to be triple donors), but on the N site they are isoelectronic and would be expected to be electronically inactive. In Fig. 3 we plot the formation energies under N-poor conditions so as to show the worst-case scenario for incorporation on the N site.

We find that P prefers to substitute on the Ge site for all chemical potentials and all Fermi levels. Examining the local relaxations we find that P_{Ge} bonds symmetrically to its four nearest-neighbor N atoms, causing a breathing relaxation as

the four P-N bond lengths contract by 10% of the bulk Ge-N bond lengths. For P_N, there is an asymmetric relaxation in the neutral state, where the P-Zn bonds are 17% longer than bulk N-Zn bonds, and the P-Ge bonds are 9% longer than bulk N-Ge bonds. These large relaxations are an indication of the size mismatch between P and N, and partially explain why, despite P being isoelectronic to N, P_N has a significantly higher formation energy than P_{Ge}. We also find P_{Zn} acts as a triple donor, but has a very high formation energy under *n*-type conditions and is unlikely to form.

As shown in Fig. 3, we find that As prefers substitution on the Ge site for most Fermi levels, but under N-poor conditions, As_N is more stable than As_{Ge} when the Fermi level is high in the gap. Conveniently, since As_N is electrically neutral under *n*-type conditions, it will not compensate As_{Ge} donors. In terms of relaxations, we find that As_{Ge} in the positive charge state causes only a small breathing relaxation where As-N bond lengths are 3% shorter than bulk Ge-N bond lengths. Similar to P_N, As_N causes a large asymmetric relaxation, where As-Zn bonds are 20% longer than bulk N-Zn bonds and As-Ge bonds are 11% longer than bulk N-Ge bonds. Lastly, like P_{Zn}, As_{Zn} acts as a donor, but under *n*-type conditions, it is unlikely to form.

Ionic radii can be used to explain the relaxations around P_{Ge} and As_{Ge} in the positive charge state. P^{5+} has an ionic radius of 0.17 Å, As^{5+} 0.34 Å, and Ge^{4+} 0.39 Å [36]. The differences in these ionic radii agree with the differences in length between the N-P, N-As, and N-Ge bond lengths to within 0.03 Å.

P and As are isovalent with N and we therefore expect them to occur in the neutral charge state. We find, however, that for Fermi levels in the lower part of the gap they can also be stable in the positive charge state. The positive charge states are associated with localized hole states. These findings are consistent with the As_N substitutional impurity in GaN [37,38].

2. Group-VI donors: S and Se

We have previously studied O as a potential unintentional dopant in Ref. [15] and found that O_N acts as a shallow donor, but O doping does not lead to high *n*-type conductivity due to effects of compensation. However, other group-VI elements such as S and Se may act as good donors. This is indeed confirmed by the results in Fig. 4, where S_N and Se_N are found to be stable only in a positive charge state. *DX* configurations are not stable; in each case, the transition level between the between the positive and negative charge states occurs well above the CBM.

The formation energies in Fig. 4 are plotted for Zn-poor conditions. Since we would like the group-VI dopants to substitute on the N site, Zn-poor (i.e., N-rich) conditions constitute a worst-case scenario for such incorporation. Even then, S_{Zn}, Se_{Zn}, S_{Ge}, and Se_{Ge} all have much higher formation energies than S_N or Se_N. Substitution on the N site is thus strongly preferred under all growth conditions. However, the formation energies of S_N and Se_N are high when E_F is high in the gap, and we will see that this leads to very low electron concentrations when *n*-type doping is attempted.

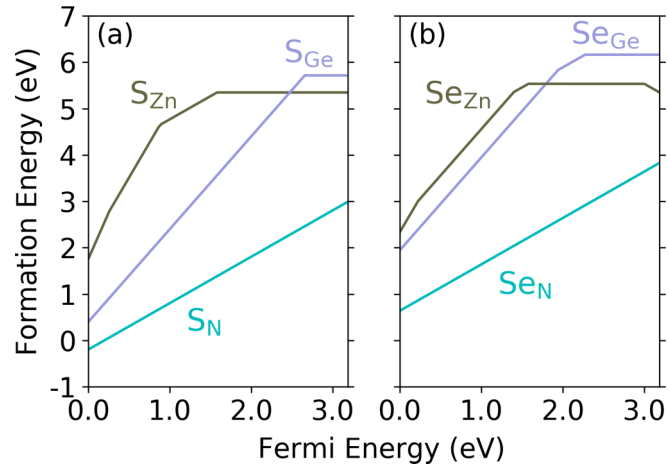

FIG. 4. Formation energies for (a) S and (b) Se substitutional impurities in $ZnGeN_2$ under Zn-poor conditions.

S_N bonds to two Zn atoms and two Ge atoms. In the positive charge state, S_N causes a large asymmetric relaxation, where S-Ge bond lengths are 19% longer than bulk N-Ge bond lengths and S-Zn bond lengths are 12% longer than bulk N-Zn bond lengths. A similar relaxation occurs for Se_N in the positive charge state, where Se-Ge bonds are 23% longer than bulk N-Ge bonds, and Se-Zn bonds are 15% longer than N-Zn bonds.

3. Carrier concentrations

We now examine the levels of *n*-type doping that can be achieved with various donor impurities. This will depend on the formation energies of the substitutional donors as well as any compensating acceptors that may form. In a previous study [15], we identified Zn_{Ge} and V_{Zn} as the dominant native acceptors in $ZnGeN_2$; V_{Ge} is much less likely to form. In Fig. 5 we plot the formation energies of these dominant acceptors alongside those of our candidate donors. We chose Zn-poor conditions, which were found to suppress the formation of native acceptors [15]. The plot shows that even under these conditions, compensation by native acceptors is a serious problem in $ZnGeN_2$. However, given that there is a lot of flexibility in choosing chemical potentials (corresponding to

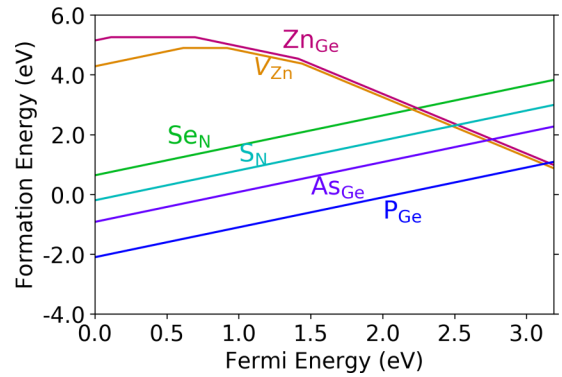

FIG. 5. Formation energies for candidate dopants and native acceptors in $ZnGeN_2$ under Zn-poor conditions.

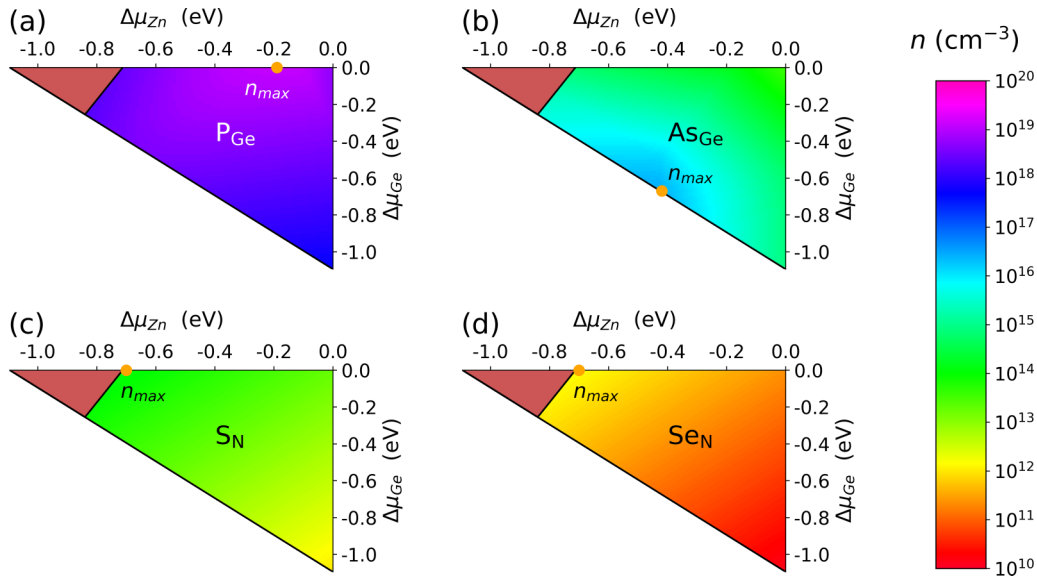

FIG. 6. Calculated electron concentration as a function of chemical potentials for $ZnGeN_2$ doped with (a) P, (b) As, (c) S, or (d) Se, for a range of chemical potentials allowed by the phase stability diagram and at a growth temperature of 1000 K. The chemical potential condition that enables the highest carrier concentration is indicated by n_{max} for each dopant.

growth under different conditions), one may wonder whether it is possible to identify conditions that would be more optimal for achieving n-type doping.

To examine this, we investigate the actual carrier concentrations that can be achieved. These depend on the concentrations of donors and acceptors in the system, which are determined by their formation energies. We have seen that these formation energies depend on the Fermi level. In an actual material, the Fermi level is fixed by the condition of charge neutrality, as expressed in Eq. (4). We perform this investigation over the full range of allowed chemical potentials, which is determined by the phase stability diagram for $ZnGeN_2$ [7,15]. This diagram shows the range of chemical potentials $\Delta\mu_i$ for each element i for which $ZnGeN_2$ is stable, in the presence of competing phases. Small changes in chemical potential can significantly change defect concentrations, due to the exponential dependence in Eq. (3). By exploring this full phase space, we are able to provide growth-condition guidelines for maximizing the electron concentration.

In Fig. 6, we use a color map to illustrate how the electron concentration depends on the chemical potential for each dopant at a growth temperature of 1000 K. The carrier concentration results from solving the charge-balance condition [Eq. (4)] quantitatively, including potential compensation by native acceptors.

Phosphorous [Fig. 6(a)] stands out as the best dopant; we find that a concentration of $n = 1.3 \times 10^{19}$ cm^{-3} can be achieved. Notably, we find that the maximum carrier concentration is found neither at the Zn-poor condition, where the formation energy of the acceptors is highest, nor at the Ge-poor condition, where the formation energy of the P_{Ge} is lowest, but somewhere in the middle, near the N-poor condition.

When doping with arsenic [Fig. 6(a)], it is possible to reach concentrations up to $n = 2 \times 10^{16}$ cm^{-3} for conditions roughly midway between the Zn-poor and Ge-poor limits. Sulfur and selenium, finally, are found to be poor dopants (which was evident already from their high formation energies, Fig. 4). Sulfur can yield concentrations up to $n = 1 \times 10^{14}$ cm^{-3}, while with selenium $n = 1 \times 10^{12}$ cm^{-3} can be achieved, both under Zn-poor conditions.

B. $ZnSiN_2$

For $ZnSiN_2$ we have performed a similar comprehensive study as presented in Sec. III A for $ZnGeN_2$, for the same set of potential dopants and analogous native acceptors (V_{Zn}, V_{Si}, and Zn_{Si}). We will present the results for the dopant configurations in less detail because, as we will show, compensation by native acceptors is an insurmountable problem in $ZnSiN_2$.

Formation energies are shown in Fig. 7. Similar to the case of $ZnGeN_2$, we find that As_{Si} has much higher formation energy than P_{Si}, and that Se_N has much higher formation energy than S_N. We have also found that Al, Ga, and In can substitute both as a donor on the Zn site or as an acceptor

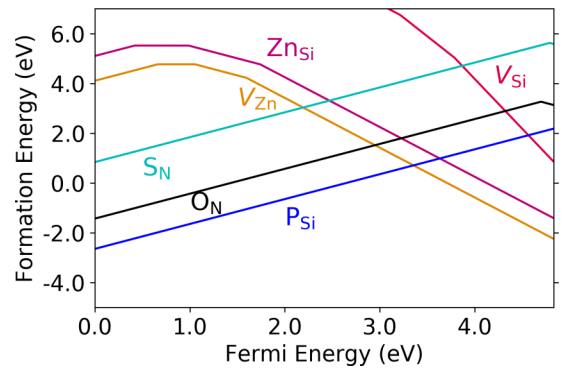

FIG. 7. Formation energies for candidate dopants and native acceptors in $ZnSiN_2$ donors and compensating acceptors under Zn-poor conditions.

on the Si sites. As a result, they self-compensate and will not lead to *n*-type doping. Therefore, we focus on P_{Si} and S_N as potential donors. We also examine O_N.

P_{Si} is a shallow donor, stable only in the +1 charge state. P_{Si} gives rise to a small breathing relaxation where the P-N bonds are 4.8% shorter than bulk Si-N bonds. The P-N bond lengths in $ZnSiN_2$ are similar to the P-N bonds in $ZnGeN_2$ (just 0.9% shorter). The P_{Si} $(+/0)$ and $(0/-)$ transition levels occur well above the CBM, indicating that P_{Si} does not exhibit *DX*-center behavior.

S_N and O_N do behave as *DX* centers, as they have a $(+/-)$ transition level within the gap. However, these transition levels are very near the CBM, 0.04 eV below the CBM for S_N and 0.13 eV below the CBM for O_N, and therefore in principle S_N and O_N can still contribute electrons to the conduction band. In the positive charge state, O_N causes an asymmetric relaxation, with O-Zn bonds 11% longer than bulk N-Zn bonds but O-Si bond lengths within 2% of bulk N-Si bonds. For S_N in the positive charge state, a similar but larger relaxation is found: S-Zn bonds are 10% longer than bulk N-Zn bonds and S-Si bonds are 21% longer than bulk N-Si bonds. This is unsurprising, considering that S has a larger ionic radius than O. However, in the negative charge states, the relaxations are different. For O_N, the O atom shifts away from a nearest-neighbor Zn atom and assumes a position in the plane formed by the other nearest-neighbor Zn atom and the two nearest-neighbor Si atoms. For S_N there is no significant change in the position of the S atom; however, one of the nearest-neighbor Si atoms moves away from the S atom by 21% of the bulk N-Si bond length.

Qualitatively the native defects in $ZnSiN_2$ behave similarly to the native defects in $ZnGeN_2$. We find V_{Si} has much higher formation energy than V_{Zn} and Zn_{Si}, similar to the high formation energy seen for V_{Ge} in $ZnGeN_2$. V_{Zn} and Zn_{Si} have properties similar to V_{Zn} and Zn_{Ge} in $ZnGeN_2$: they both have low formation energies in the −2 charge state under *n*-type conditions. Furthermore, the positions of the transition levels of V_{Zn} and Zn_{Si} within the band gap of $ZnSiN_2$ are very similar to those of V_{Zn} and Zn_{Ge} in $ZnGeN_2$ when the band alignment between the two materials is taken into account [39].

A significant difference between the native defects in $ZnGeN_2$ and $ZnSiN_2$ is that the formation energy of V_{Zn} is much lower in $ZnSiN_2$ than in $ZnGeN_2$. In particular, the formation energy of V_{Zn} is negative for the Fermi level at the CBM for any choice of chemical potentials. As a result, V_{Zn} would spontaneously form in any *n*-type $ZnSiN_2$. An analysis comparable to Fig. 6 indicates that the maximum carrier concentration achievable in $ZnSiN_2$ is on the order of a few times 10^{13} cm^{-3}, and therefore *n*-type conductivity cannot be achieved.

IV. SUMMARY

We have investigated a variety of potential donors in $ZnGeN_2$ and $ZnSiN_2$. For $ZnGeN_2$ we find S_N, Se_N, P_{Ge}, and As_{Ge} to act as shallow donors. However, compensation by the native Zn_{Ge} and V_{Zn} acceptors can hamper doping. We identify P_{Ge} as the best donor: *n*-type carrier concentrations up to 1.3×10^{19} cm^{-3} may be achieved under N-poor conditions.

In the wider-band-gap $ZnSiN_2$, we find the native acceptors have qualitatively similar behaviors as in $ZnGeN_2$. P_{Si} acts a shallow donor, while S_N and O_N have transitions to the negative charge state near the CBM. However, compensation by native acceptors is very strong in $ZnSiN_2$, indicating that *n*-type doping is not possible.

ACKNOWLEDGMENTS

This work was supported by the Army Research Office (Grant No. W911NF-16-1-0538). Work by D.W. on $ZnGeN_2$ was supported by the US Department of Energy (DOE), Office of Science, Basic Energy Sciences (BES) under Award No. DE-SC0010689 and work by D.W. on $ZnSiN_2$ was supported by a National Research Council Fellowship at the US Naval Research Laboratory. Computational resources were provided by the Extreme Science and Engineering Discovery Environment (XSEDE) [supported by National Science Foundation (NSF) Grant No. ACI-1548562], by the Department of Defense High Performance Computing Modernization Program at the Army Research Office/Office of Naval Research (Project No. ARONC4175), and by the Center for Scientific Computing, which is supported by the California NanoSystems Institute and the Materials Research Science and Engineering Center (MRSEC) at UC Santa Barbara through Grants No. NSF DMR-1720256 and No. NSF CNS-1725797.

[1] A. D. Martinez, A. N. Fioretti, E. S. Toberer, and A. C. Tamboli, J. Mater. Chem. A **5**, 11418 (2017).

[2] P. C. Quayle, K. He, J. Shan, and K. Kash, MRS Commun. **3**, 135 (2013).

[3] A. Osinsky, V. Fuflyigin, L. D. Zhu, A. B. Goulakov, J. W. Graff, and E. F. Schubert, in *Proceedings 2000 IEEE/Cornell Conference on High Performance Devices (Cat. No.00CH37122)* (IEEE, New York, 2000), pp. 168–172.

[4] L. Han, C. Lieberman, and H. Zhao, J. Appl. Phys. **121**, 093101 (2017).

[5] T. Misaki, A. Wakahara, H. Okada, and A. Yoshida, J. Cryst. Growth **260**, 125 (2004).

[6] L. Lahourcade, N. C. Coronel, K. T. Delaney, S. K. Shukla, N. A. Spaldin, and H. A. Atwater, Adv. Mater. **25**, 2562 (2013).

[7] S. Chen, P. Narang, H. A. Atwater, and L.-W. Wang, Adv. Mater. **26**, 311 (2014).

[8] T. D. Veal, N. Feldberg, N. F. Quackenbush, W. M. Linhart, D. O. Scanlon, L. F. J. Piper, and S. M. Durbin, Adv. Energy Mater. **5**, 1501462 (2015).

[9] A. M. Shing, N. C. Coronel, N. S. Lewis, and H. A. Atwater, APL Mater. **3**, 076104 (2015).

[10] S. Kikkawa and H. Morisaka, Solid State Commun. **112**, 513 (1999).

[11] T. Endo, Y. Sato, H. Takizawa, and M. Shimada, J. Mater. Sci. Lett. **11**, 424 (1992).

[12] N. Tsunoda, Y. Kumagai, A. Takahashi, and F. Oba, Phys. Rev. Appl. **10**, 011001 (2018).
[13] A. N. Fioretti, A. Zakutayev, H. Moutinho, C. Melamed, J. D. Perkins, A. G. Norman, M. Al-Jassim, E. S. Toberer, and A. C. Tamboli, J. Mater. Chem. C **3**, 11017 (2015).
[14] D. Skachkov, A. Punya Jaroenjittichai, L.-y. Huang, and W. R. L. Lambrecht, Phys. Rev. B **93**, 155202 (2016).
[15] N. L. Adamski, Z. Zhu, D. Wickramaratne, and C. G. Van de Walle, J. Appl. Phys. **122**, 195701 (2017).
[16] L. Gordon, J. B. Varley, J. L. Lyons, A. Janotti, and C. G. Van de Walle, Phys. Status Solidi Rapid Res. Lett. **9**, 462 (2015).
[17] J. S. Harris, J. N. Baker, B. E. Gaddy, I. Bryan, Z. Bryan, K. J. Mirrielees, P. Reddy, R. Collazo, Z. Sitar, and D. L. Irving, Appl. Phys. Lett. **112**, 152101 (2018).
[18] N. L. Adamski, Z. Zhu, D. Wickramaratne, and C. G. Van de Walle, Appl. Phys. Lett. **114**, 032101 (2019).
[19] P. E. Blöchl, Phys. Rev. B **50**, 17953 (1994).
[20] G. Kresse and J. Furthmüller, Phys. Rev. B **54**, 11169 (1996).
[21] G. Kresse and J. Furthmüller, Comput. Mater. Sci. **6**, 15 (1996).
[22] J. Heyd, G. E. Scuseria, and M. Ernzerhof, J. Chem. Phys. **118**, 8207 (2003).
[23] M. Wintenberger, M. Maunaye, and Y. Laurent, Mater. Res. Bull. **8**, 1049 (1973).
[24] H. Jonas, S. Saskia, W. Peter, and S. Wolfgang, Chem. Eur. J **23**, 12275 (2017).
[25] A. Punya, W. R. L. Lambrecht, and M. van Schilfgaarde, Phys. Rev. B **84**, 165204 (2011).
[26] C. Freysoldt, B. Grabowski, T. Hickel, J. Neugebauer, G. Kresse, A. Janotti, and C. G. Van de Walle, Rev. Mod. Phys. **86**, 253 (2014).
[27] C. Freysoldt, J. Neugebauer, and C. G. Van de Walle, Phys. Rev. Lett. **102**, 016402 (2009).
[28] C. Freysoldt, J. Neugebauer, and C. G. Van de Walle, Phys. Status Solidi B **248**, 1067 (2011).
[29] D. D. Wagman, W. H. Evans, and V. B. Parker, *The NBS Tables of Chemical Thermodynamic Properties: Selected Values for Inorganic and C1 and C2 Organic Substances in SI Units* (American Chemical Society and American Institute of Physics for the National Bureau of Standards, New York, 1982).
[30] C. Qin, L. Gao, and E. Wang, in *Encyclopedia of Inorganic Chemistry*, edited by R. A. Scott (John Wiley & Sons, New York, 2011).
[31] P. O'Hare, I. Tomaszkiewicz, I. C. M. Beck, and H.-J. Seifert, J. Chem. Thermodyn. **31**, 303 (1999).
[32] A. Nasar and M. Shamsuddin, Thermochim. Acta **205**, 157 (1992).
[33] M. W. Chase, *NIST-JANAF Thermochemical Tables*, 4th ed. (American Institute of Physics, Woodbury, NY, 1998).
[34] R. C. Schoonmaker, A. R. Venkitaraman, and P. K. Lee, J. Phys. Chem. **71**, 2676 (1967).
[35] A. S. Jordan, J. Electrochem. Soc. **118**, 1362 (1971).
[36] R. D. Shannon, Acta Crystallogr. A **32**, 751 (1976).
[37] T. Mattila and A. Zunger, Phys. Rev. B **58**, 1367 (1998).
[38] C. G. Van de Walle and J. Neugebauer, Appl. Phys. Lett. **76**, 1009 (2000).
[39] N. L. Adamski, D. Wickramaratne, and C. G. Van de Walle (unpublished) .